THE JOURNAL OF PHYSICAL CHEMISTRY B

Article

pubs.acs.org/JPCB

Modulation of Photophysics and Photodynamics of 1′-Hydroxy-2′-acetonaphthone (HAN) in Bile Salt Aggregates: A Study of Polarity and Nanoconfinement Effects

Sarthak Mandal, Surajit Ghosh, Chiranjib Banerjee, Vishal Govind Rao, and Nilmoni Sarkar*

Department of Chemistry, Indian Institute of Technology, Kharagpur 721302, WB, India

Supporting Information

ABSTRACT: The modulation of the photophysical properties of 1′-hydroxy-2′-acetonaphthone (HAN) upon encapsulation into the hydrophobic nanocavities of different bile salt aggregates has been investigated for the first time using steady-state and time-resolved fluorescence spectroscopy. Because HAN is very sensitive to the polarity of the microenvironment in which it is confined, we performed a comparative study on the excited-state binding dynamics of HAN using three different bile salts of varying hydrophobicity. The encapsulation of HAN into the bile salt aggregates led to an enhanced fluorescence intensity along with a significant blue shift in the emission maxima that was highly sensitive to the confined microenvironment. Using HAN as a sensitive fluorophore to probe the nanocavities of bile salt aggregates in aqueous solution, we found different mechanisms of probe encapsulation depending on the degree of hydrophobicity of the nanocavities, which results in a difference in the alteration of the spectral behavior. A sharp increase in the fluorescence quantum yield near the cmc was observed, followed by saturation for all three bile salt aggregates. However, maximum fluorescence quantum yield in NaDC aggregates can be rationalized by maximum partitioning of HAN into the more hydrophobic and rigid environment provided by NaDC aggregates. Moreover, the alteration of the spectral behavior with increasing concentration of bile salts strikingly differs from that observed previously in the presence of conventional surfactants. Time-resolved fluorescence measurements further elucidated how the probe molecules interact with the aggregates. Longer fluorescence lifetime and anisotropy values clearly indicate the caging of the tautomers of HAN into the hydrophobic nanocavities of bile salt aggregates. This work further demonstrates the changes in the fluorescence properties of HAN with structural changes of bile salt aggregates induced by the addition of salt and organic cosolvent.

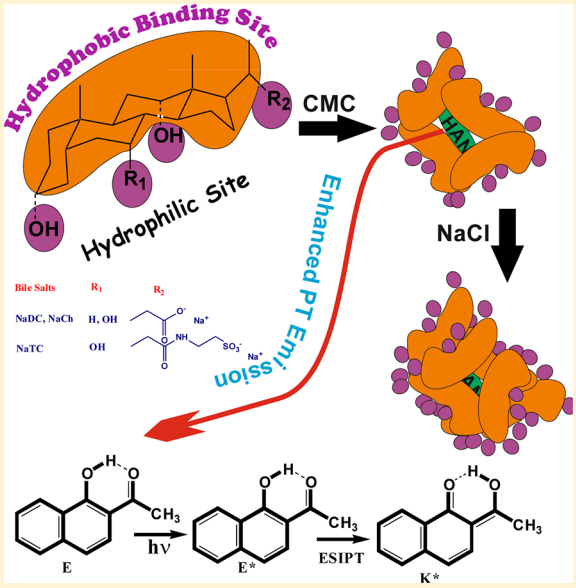

1. INTRODUCTION

Bile salts, the most widely studied naturally occurring amphiphilic compounds, are of great interest to the research communities of chemistry and biology because of their unique roles in a wide variety of biological processes such as solubilization of fats and other fat-soluble substances in living organisms.[1−3] Understanding the binding dynamics of guest molecules confined within the nanocavities of various chemically and biologically active supramolecular host systems has been the subject of active scientific research for the past several years.[4−8] In this time, the importance of host−guest inclusion complexes has been demonstrated for a variety of chemical, biological, and industrial applications, including the development of drug-delivery systems,[9] energy-storage materials and devices, photonic devices, and nanometer-sized electronic devices.[10] Bile salt aggregates are potential supramolecular host systems that can carry both hydrophobic and hydrophilic guest molecules of suitable size and shape because of the presence of both types of binding sites under varying experimental conditions, such as concentration, pH, and ionic strength of the surrounding medium.[11−13] The self-assemblies of bile salts are of particular interest from the biological point of view because of their unique ability to solubilize various biologically active organic guests including many sparingly water-soluble drug molecules.[14−18] Moreover, the formation of inclusion complexes in such aggregates helps to control the selectivity of various chemical reactions such as photoinduced reactions, enzymatic reactions, and complexation reactions.[19,20] Unlike common surfactant molecules, bile salts have a nonplanar steroidal skeleton with a convex surface of

Received: March 13, 2012
Revised: May 23, 2012
Published: June 15, 2012

   dx.doi.org/10.1021/jp302435h | J. Phys. Chem. B 2012, 116, 8780−8792

hydrophobic groups and a concave surface of hydrophilic groups. Several studies have been performed to understand the aggregation behavior of bile salts in solution, and the aggregation behavior is reported to be more complex in nature than that of conventional surfactant molecules.[21] Among the several models proposed to explain the aggregation of bile salts in solution, the primary and secondary aggregate model proposed by Small and colleagues[1,22] is the most widely accepted one. According to this model, primary aggregates of 2−10 monomers where the hydrophilic groups point outward are formed at low bile salt concentrations because of the hydrophobic interactions of the convex surfaces of the monomers. Primary aggregates are reported to be very useful for selective binding of hydrophobic probe molecules into their nanocavities.[11−13] In another model, the aggregation behavior of bile salts is said to be governed by hydrogen-bonding interactions between the bile salt monomers.[23] Many theoretical[24] and experimental[25] studies have shown that both hydrophobic and hydrogen-bonding interactions play significant roles during the formation of primary aggregates. As the concentration of monomer is increased, primary aggregates are agglomerated into secondary aggregates in which the hydrophilic probe molecules are preferentially solubilized in the hydrophilic core filled with water.

Recently, Baldridge et al.[26] demonstrated the turn-on fluorescence of fluorescent protein chromophores such as (arylmethylene)imidazolinones (AMIs) of varying substituents (hydrophobic/hydrophilic) through encapsulation in NaCh aggregates. Bohne and co-workers[11−13] extensively studied the binding dynamics of various organic guest molecules in the hydrophobic nanocavities of bile salt aggregates using fluorescence and other spectroscopic studies. In addition, different ultrafast fluorescence-based techniques including fluorescence resonance energy transfer (FRET),[27] solvation dynamics,[28] and photoinduced electron transfer (PET)[29] have been performed under the restricted microenvironment of bile salt aggregates to obtain a better understanding of the excited-state dynamics of the confined probe molecules. Moreover, the different regions of bile salt aggregates were recently probed by Adhikari et al.[30] using excitation-wavelength-dependent femtosecond solvation dynamics study. Whereas substantial efforts have been made to study the binding dynamics of various organic guests within the nanocavities of bile salt aggregates, much less attention has been paid to the binding interaction of the proton-transferred (PT) probe molecules despite their potential range of applications including the development of white light-emitting diodes, proton-transfer lasers, and photostabilizers.[31,32]

The probe molecules, which undergo an intramolecular or intermolecular proton-transfer process, are usually referred to as PT probe molecules. The excited-state proton-transfer (ESPT) process, one of the fundamental reactions in photochemistry, was first observed by Weller in 1952.[33−35] Since then, many theoretical and experimental studies have been performed using various proton-transfer probe molecules to understand the PT dynamics in both homogeneous and heterogeneous media.[36−44] However, studies on the PT dynamics of 1′-hydroxy-2′-acetonaphthone (HAN), which has potential polymer-protection capabilities,[45] are insufficient. The aromatic compound 1′-hydroxy-2′-acetonaphthone (HAN) is known as an excited-state intramolecular proton-transfer (ESIPT) probe molecule with a strong intramolecular hydrogen bond in the ground state.[46] Such molecules with strong intramolecular hydrogen bonds are of great interest not only because of their involvement in the ESIPT process but mainly because of their potential ability to respond to changes in their microenvironment, which helps to make them sensitive probes for biomolecular cavity environments such as protein cavities. Catalán et al.[47] showed that HAN could be a good candidate for obtaining information about the hydrophobicity, polarity, and polarizability of the concave face of supramolecular assemblies.

In 1993, Douhal et al.[48] first described that the dual fluorescence of HAN under free-jet expansion condition originates from the involvement of the ESIPT process where the short- and long-wavelength emissions are attributed to the enol (E*) and keto (K*) forms, respectively (Scheme 1). Since

Scheme 1. Schematic Representation of the Different Tautomers of HAN Involved in the ESIPT Process of HAN

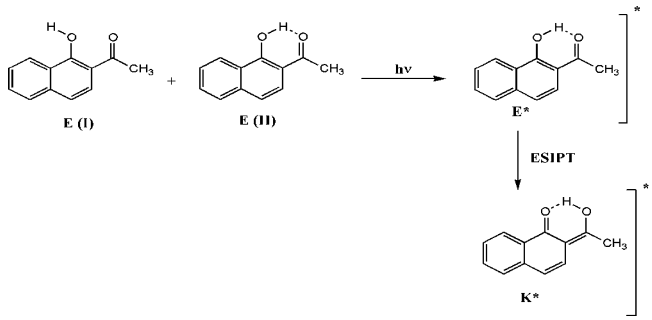

then, many theoretical[46,49,50] and experimental[51−55] studies have been performed on the proton-transfer dynamics of HAN. The Cheng group[54] reported earlier that proton transfer of HAN occurs on the picosecond time scale. However, on the basis of femtosecond time-resolved transient absorption experiments, Lochbruner et al.[51] suggested that PT occurs on the time scale of ∼30 fs. Using laser photolysis and the time-resolved thermal lensing technique, Tobita et al.[55] studied the effect of electronic structure on the ESIPT process in HAN and its structural analogues, HNA (1-hydroxy-2-naphthaldehyde) and HMN (methyl-1-hydroxy-2-naphthoate). In their work, the Stokes-shifted emissions of HAN and HNA were assigned to the proton-transferred keto form, suggesting the involvement of the PT reaction in HAN and HNA but not in HMN. However, Catalán et al.[56−58] did not recognize the involvement of the PT process in HAN. Guchhait and colleagues[59−61] extensively studied the photophysical properties of HNA in different homogeneous and heterogeneous systems and concluded that the fluorescence emission of HNA originates from the major contributing proton-transferred keto tautomer. In line with their observations, many other groups have reported that the fluorescence emission of HAN in aprotic solvents originates from the proton-transferred keto form.[50,54,62] However, many theoretical studies[46,53,63] have predicted that the keto tautomer of HAN does not exhibit any energy minima in the ground electronic state. This implies that the structured emission of HAN as observed by Catalán et al.[58] does not originate from the keto tautomer. Therefore, to explain the structured emission, Organero et al.[46,49] suggested the formation of a rotamer (which they denoted KR*) in the excited state from the proton-transferred keto tautomer. They further concluded that this rotamer is more stable than the keto tautomer in the first singlet excited state and that it has energy minima in the

dx.doi.org/10.1021/jp302435h | J. Phys. Chem. B 2012, 116, 8780−8792

ground electronic state. Recently, however, Ortiz-Sánchez et al.[50] used an improved level of theoretical calculations to show that KR* structures are more unstable than the keto tautomer. Very recently, on the basis their theoretical observations, Catalán et al.[58] discarded the existence of KR*. They further proposed that, upon photoexcitation, HAN exhibits two stable enol forms of similar energies, both of which are emissive and can easily reconvert in the first singlet excited state. The new enol form in which the methyl group is staggered with respect to its carbonyl oxygen might result in the formation of a keto tautomer after proton transfer or an alternative form with a strongly deformed chelate ring. There is still some confusion as to whether the emission of HAN originates from the enol form or the proton-transferred keto form.

Extensive studies have been performed on the excited-state proton-transfer dynamics of HAN in neat homogeneous solution, and the effects of temperature, viscosity, H-bonding ability, and polarity of the solvents have been reported.[64] Catalán et al.[47] observed that the larger the polarity of the solvent, the larger the red shift in the emission spectrum of HAN. In neat aqueous solution, the Stokes-shifted emission of HAN appears at ∼490 nm. However, in nonpolar aprotic solvents such as cyclohexane and methylcyclohexane, HAN exhibits a broad structured emission with a maximum centered at 480 nm and a hump at 450 nm.[5,62] The excitation spectra of HAN in cyclohexane monitored at emission wavelengths of 450 and 480 nm correlate well with the absorption spectrum. Moreover, Catalán and de Paz[58] observed that, at low temperature, the first absorption band of HAN in 2-methylbutane strongly resembled the emission spectrum. These observations help to point out that the emission of HAN originates from the similar species that absorbs at ∼368 nm in the ground state and the only ground-state species that absorbs at ∼368 nm is assigned to the intramolecularly hydrogen-bonded closed enol conformer.

In neat aqueous solution, the Stokes-shifted emission at 490 nm is blue-shifted with a significant enhancement in emission intensity upon confinement within the hydrophobic nanocavities of different supramolecular assemblies such as micelles, vesicles, cyclodextrins, modified cyclodextrins, and human serum albumin (HSA).[65−69] The binding interaction and location of HAN in such self-assembled biomimicking organized systems has been studied using steady-state and time-resolved fluorescence spectroscopy.[65−68] However, no systematic study has been performed on the modulation of the PT dynamics of HAN in the hydrophobic nanocavities of different bile salt aggregates, even though such aggregates are known to affect the excited-state dynamics of aggregate-bound probe molecules in a significant way.[27−30] Regarding the PT dynamics inside bile salt aggregates, very recently, Selvam et al.[70] studied the ESIPT process of fisetin, a class of flavonoids in sodium cholate aggregates. In the present work, we explored HAN as a sensitive fluorophore to probe bile salt aggregates and investigated the effect of nanoconfinement on the proton-transfer dynamics of HAN. Using three different bile salts of varying hydrophobicity, we found that HAN is very sensitive to the binding-site polarity of the systems. In addition to the microenvironmental parameters, this work helps to understand the location and distribution of probe molecules in such biologically important microheterogeneous systems, which are capable of carrying a number of sparingly water-soluble hydrophobic drug molecules. Moreover, we demonstrate the changes in the fluorescence properties of HAN with the structural changes of the bile salt aggregates induced by the addition of salt and organic cosolvent.

2. EXPERIMENTAL SECTION

2.1. Chemicals. 1′-Hydroxy-2′-acetonaphthone (HAN) was purchased from Sigma Aldrich and used as received. The different bile salts, namely, NaDC, NaC, and NaTC, were also purchased from Sigma Aldrich and used as received. Dimethylformamide (DMF, HPLC-grade; Merck) and NaCl (Sigma Aldrich) were used as received. The structures of all three bile salts used in these experiments are presented in Scheme 2.

Scheme 2. Chemical Structures of Sodium Cholate (NaCh), Sodium Deoxycholate (NaDC), and Sodium Taurocholate (NaTC)

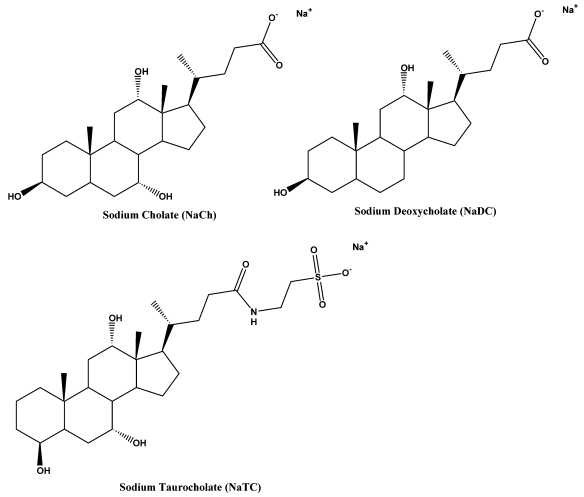

2.2. Instruments and Methods. Steady-state absorption and emission spectra were recorded on a Shimadzu (model UV 1601) UV−vis spectrophotometer and a Spex Fluorolog-3 (model FL3-11) spectrofluorimeter. In all experiments, the concentration of HAN was kept at ∼10^{-5} M. Doubly distilled Mili-Q water was used to prepare the solutions for experiments. Time-resolved emission spectra were recorded using a time-correlated single-photon-counting (TCSPC) picosecond spectrometer. The details of the experimental setup for picosecond TCSPC spectrometry is described in our previous work.[71] In brief, a picosecond diode laser at 375 nm (NanoLED; IBH, Glasgow, Scotland) was used as the light source, and the signal was detected at magic-angle (54.7°) polarization using a Hamamastsu microchannel plate (MCP) photomultiplier tube (PMT; 3809U). The typical instrument response function is 100 ps in our system. The same setup was used for anisotropy measurements. For the anisotropy decays, we used a motorized polarizer in the emission side. The emission intensities at parallel ($I_{||}$) and perpendicular ($I_{\perp}$) polarizations were collected alternatively until a certain peak difference (i.e., the difference in the counts) between parallel ($I_{||}$) and perpendicular ($I_{\perp}$) decays was reached. The time-resolved fluorescence decays were analyzed using IBH DAS-6 decay analysis software. Bile salt solutions can contain small amounts of fluorescent impurities (Figure S5, Supporting Information). Therefore a small percentage in the contribution of the decay components of HAN in bile salt aggregates, especially at higher

dx.doi.org/10.1021/jp302435h | J. Phys. Chem. B 2012, 116, 8780−8792

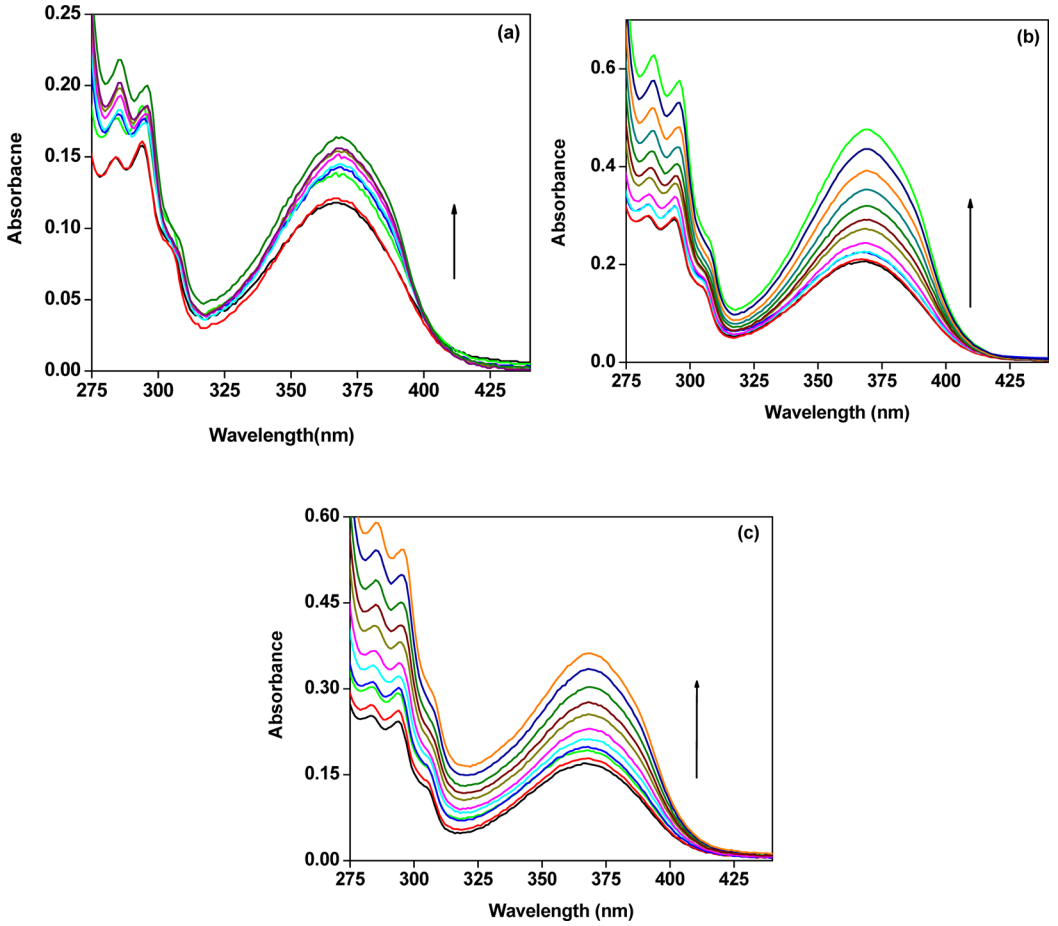

Figure 1. Absorption spectra of HAN in aqueous solution with increasing concentration of bile salts: (a) NaDC (0−15.29 mM), (b) NaCh (0−31 mM), and (c) NaTC (0−30 mM).

concentrations (40 and 80 mM), could arise from the fluorescence impurities present in the bile salts.

The same software was also used for time-resolved anisotropy decay analysis. The anisotropy decay function, $r(t)$, was constructed from the $I_{\parallel}$ and $I_{\perp}$ decays using the equation

$$r(t) = \frac{I_{\parallel}(t) - GI_{\perp}(t)}{I_{\parallel}(t) + 2GI_{\perp}(t)} \quad (1)$$

where G is the correction factor for detector sensitivity to the polarization direction of the emission and $I_{\parallel}(t)$ and $I_{\perp}(t)$ are the fluorescence decays polarized parallel and perpendicular, respectively, to the polarization of the excitation light.

The fluorescence quantum yields of HAN in different systems were determined using anthracene (λ_{abs} = 350 nm) with an absolute quantum yield of 0.27 in methanol at 25 °C as the secondary standard. The following equation was used for the calculation

$$\frac{\Phi_S}{\Phi_R} = \frac{A_S}{A_R}\frac{(\mathrm{Abs})_R}{(\mathrm{Abs})_S}\frac{{n_S}^2}{{n_R}^2} \quad (2)$$

where Φ represents the quantum yield, Abs represents absorbance, A represents the area under the fluorescence curve, and n is the refractive index of the medium. The subscripts S and R denote the corresponding parameters for the sample and reference, respectively.

2.3. Sample Preparation. Bile salt solutions were prepared by dissolving the bile salts separately in aqueous 0.2 M NaCl solution. The stock solutions of bile salts, especially for concentrated solutions, were heated at 50 °C to avoid the probability of gel formation. Then, the calculated amount of stock methanolic solution of HAN was taken in a volumetric flask so that ultimate concentration became ∼10^{-5} M for a specific volume of bile salt solution. After the methanol had been completely removed, a specific volume of stock bile salt solution was added into the flask and the solution was kept for few hours for the encapsulation of dye in the microenvironment of bile salt aggregates.

3. RESULTS

3.1. Effects of Structure and Concentration of Bile Salts. *3.1.1. Steady-State Absorption and Emission Studies.* As reported earlier, the absorption band at ∼368 nm corresponds to the intramolecularly hydrogen-bonded closed enol conformer (E-II) of HAN in the ground state. However, in aqueous solution, weakening of the intramolecular hydrogen bond can result in the formation of an additional band shifted to shorter wavelength for the open enol conformer (E-I). This possibility is supported by the theoretical prediction of Douhal et al.[46] that two water molecules can break the internal hydrogen bond of HAN. In addition, the existence of the open enol conformer can also be supported by the observation of Singh et al.[61] that the absorption band at ∼300 nm is due to the open conformer of HNA, an analogous structure of HAN

dx.doi.org/10.1021/jp302435h | J. Phys. Chem. B 2012, 116, 8780−8792

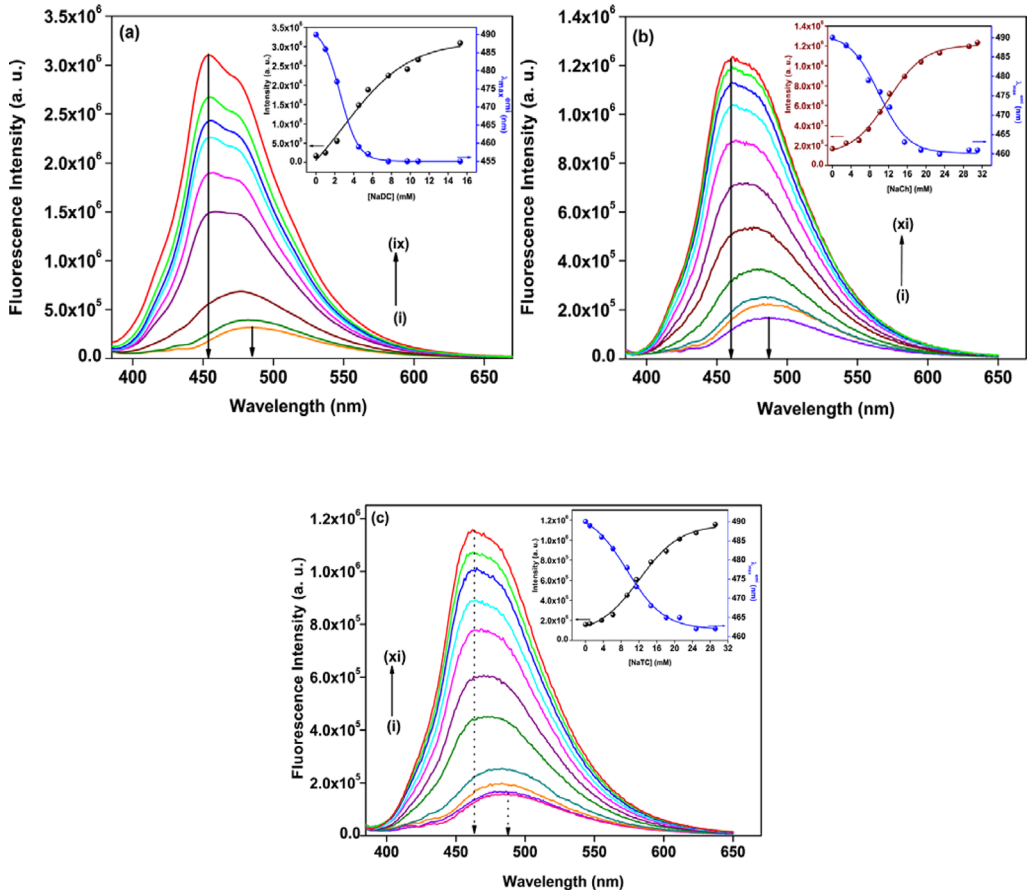

Figure 2. Emission spectra of HAN in the presence of increasing concentrations of (a) NaDC (curves i–ix correspond to NaDC concentrations of 0, 1, 2.23, 4.53, 5.53, 7.68, 9.68, 10.83, and 15.29 mM, respectively), (b) NaCh (curves i–xi correspond to NaCh concentrations of 0, 3, 5.69, 7.69, 10.15, 12.23, 15.46, 18.92, 22.92, 29.23, and 31 mM, respectively), and (c) NaTC (curves i–xi correspond to concentration of NaTC = 0, 1, 3.62, 6.12, 9.37, 11.50, 14.75, 18.12, 21.12, 24.87, and 30 mM, respectively). The insets show the variations of emission intensity at λ_{em} = 480 nm and λ_{max}^{emi} of HAN with bile salt concentration.

having similar spectral behavior.[55] Gradual addition of bile salts (NaDC/NaCh/NaTC) to the aqueous solution of HAN results in an increase of the absorbance at ~368 nm, as is evident from Figure 1. Moreover, the absorption band is slightly red-shifted (Figure S1, Supporting Information) upon encapsulation into the hydrophobic nanocavities of different bile salt aggregates, as observed in the case of binding with other hydrophobic nanocavities such as HSA and cyclodextrins.[66−68] The corresponding absorption spectra of HAN in water and cyclohexane are also included in the Supporting Information for comparison. A quantitative estimation of the partition coefficient can be made from the UV−vis difference spectra as described in our previous report for the partitioning of HAN in nonionic surfactants forming vesicles.[69]

The steady-state fluorescence spectra of HAN in aqueous 0.2 M NaCl solution with increasing concentrations of different bile salts were recorded at an excitation wavelength of 375 nm, and the corresponding changes in the fluorescence behavior are presented in Figure 2. The insets of Figure 2 are show the variations of the emission intensity and emission maxima as functions of bile salt concentration. Upon gradual addition of bile salts, significant enhancements in intensity and blue shifts of the emission maxima are observed, indicating the modulation of the excited-state dynamics as a result of the formation of host−guest inclusion complexes. Such inclusion of a hydrophobic chromophore in the hydrophobic binding site can be understood from the similar spectroscopic alteration in nonopolar solvents such as cyclohexane and methylcyclohexane compared to water.[5,62]

3.1.2. Partitioning of HAN in Different Bile Salt Aggregates. The measurable spectral changes observed in the steady-state absorption and fluorescence studies of HAN in aqueous solution with increasing concentration of bile salts due to HAN−bile salt interactions reflect significant partitioning of HAN into the hydrophobic nanocavities of bile salt aggregates. However, at this stage, it is very important to have a quantitative idea of the extent of penetration, which varies for the different types of microenvironments provided by different bile salts. The partition coefficient of a solute between two different phases can be defined as[72]

$$K_p \frac{\left(\frac{C_m}{C_t}\right)\Big/[\text{bile salt}]}{\left(\frac{C_w}{C_t}\right)\Big/[\text{water}]} \quad (3)$$

where C_t is the total concentration of HAN and C_m and C_w represent the probe concentrations in bile salt aggregates and water, respectively. Experimentally, the partition coefficient can be determined from the fluorescence spectra of HAN in aqueous solution with increasing concentration of different bile salts using the equation

dx.doi.org/10.1021/jp302435h | J. Phys. Chem. B 2012, 116, 8780−8792

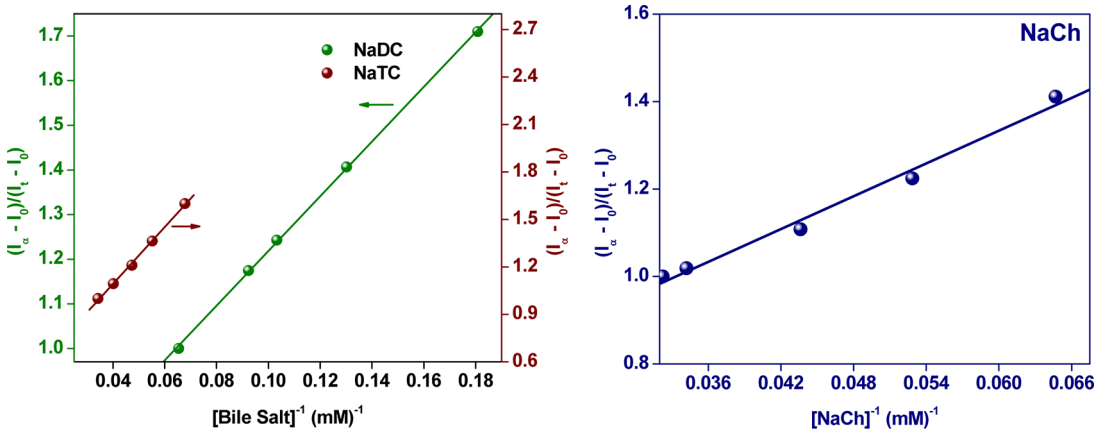

Figure 3. Plots of $(I_\infty - I_0)/(I_t - I_0)$ versus (a) $[NaDC]^{-1}$ and $[NaTC]^{-1}$, and (b) $[NaCh]^{-1}$.

$$\frac{I_\infty - I_0}{I_t - I_0} = 1 + \frac{[\text{water}]}{K_P}\frac{1}{[\text{bile salt}]} \quad (4)$$

where I_0, I_t, and I_∞ are the emission intensities of the probe molecule in the absence of surfactant (i.e., in pure water), at different concentrations above the critical micelle concentration (cmc) range of the corresponding bile salts, and at saturation. K_P is the partition coefficient of HAN to the bile salt aggregates from the bulk water. Figure 3 presents linear plots of $(I_\infty - I_0)/(I_t - I_0)$ versus the inverse of the bile salt concentration ($[\text{bile salt}]^{-1}$) for three different types of bile salt aggregates. The partition coefficients were calculated from the slope of the corresponding plot, and the values are given in Table 1. The corresponding free energy values for the complexation of HAN with the aggregates were calculated from the obtained partition coefficient values and are included in Table 1. Analysis of the results reveals that HAN exhibits quite high partition coefficients for all three bile salts.

Table 1. Partition Coefficients (K_P) and Free Energy Changes for the Complexation of HAN with Different Bile Salt Aggregates

bile salt	partition coefficient, K_P (10^3)	binding energy, $-\Delta G$ (kJ mol^{-1})
NaDC	9.06	22.56
NaCh	4.44	20.80
NaTC	3.09	19.90

3.1.3. Time-Resolved Emission Studies. In addition to steady-state observations, time-resolved fluorescence measurements are necessary to obtain better insight into the origin of the altered photophysics of HAN as a result of nanoconfinement within bile salt aggregates. Time-resolved fluorescence decays of HAN in aqueous 0.2 M NaCl solutions with varying concentrations of different bile salts were recorded at an excitation wavelength of 375 nm and monitored at an emission wavelength of 480 nm using a time-correlated single-photon-counting (TCSPC) device, and the corresponding decay profiles are given in Figure 4. The decay parameters obtained from the best exponential fitting of the fluorescence decays are listed in Table 2. In neat aqueous solution, biexponential fluorescence decay was observed with time constants of ~90 ps (99%) and ~4 ns (1%), consistent with previous literature reports.[64−68] The major contributing fast component is assigned to the proton-transferred (PT) keto form (K*), and the minor contributing slow component is due to the open enol conformer of HAN.[50,54,59,60,62] Addition of bile salt leads to triexponential behavior of the fluorescence decays; for example, in an aqueous solution of 20 mM NaDC, the lifetime values were 110 ps (43%), 510 ps (55%), and 1.89 ns (2%), where the values in parentheses indicate the percentage relative contributions. The fast component is attributed to the free HAN present in the aqueous phase, whereas the other two components of longer lifetime (picosecond and nanosecond) are attributed to the caged tautomers of HAN. The relative contribution of the fast component gradually decreased with increasing concentration of bile salt, which is an indication of probe encapsulation. However, when the concentration of the bile salt changed from 40 to 80 mM, a marked increase in the relative contribution of the fast component was observed, which probably arose because of the small percentage contribution (Figure S5, Supporting Information) from the fluorescence impurities present in bile salts of higher concentration.

Therefore, not giving too much emphasis on the individual components of the fluorescence lifetime values in such complex biological systems, we calculated the average fluorescence lifetime to explain the excited-state binding dynamics of HAN. The changes in the fluorescence lifetime values with gradual addition of bile salts help to provide an idea about the modulation of radiative and nanoradiative decay processes through the encapsulation of the probe molecules. The radiative and nonradiative decay rate constants were calculated from the determined fluorescence quantum yields and average fluorescence lifetimes using the equations

$$k_r = \frac{\Phi_f}{\langle \tau_f \rangle} \quad (5)$$

$$k_{nr} = \frac{1}{\langle \tau_f \rangle} - k_r \quad (6)$$

where k_r and k_{nr} represent the radiative and nonradiative rate constants, respectively. The calculated values are reported in Table 2. A gradual decrease in the nonradiative rate constant values of HAN in aqueous solution of constant ionic strength was observed with increasing concentration of bile salts because of the reduced degree of rotational and vibrational relaxation of the PT tautomer upon confinement in the hydrophobic pockets of bile salt aggregates.

3.1.4. Time-Resolved Anisotropy Studies. Time-resolved anisotropy studies shed further light on the microenvironment

dx.doi.org/10.1021/jp302435h | J. Phys. Chem. B 2012, 116, 8780−8792

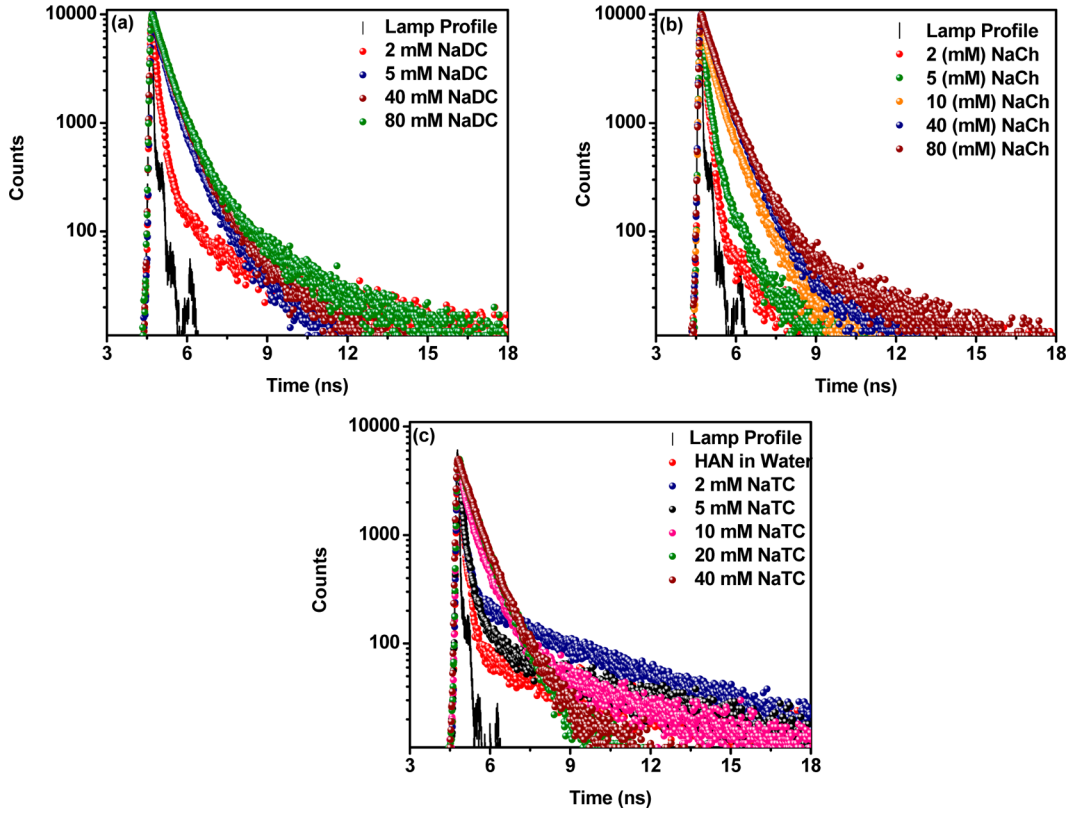

Figure 4. Time-resolved fluorescence decay of HAN in aqueous 0.2 M NaCl solutions of (a) NaDC, (b) NaCh, and (c) NaTC with increasing concentrations (λ_{ex} = 375 nm, λ_{em} = 480 nm).

Table 2. Fluorescence Lifetimes and Quantum Yields (Φ_f) and Radiative and Nonradiative Rate Constants of HAN in Aqueous (0.2 M) NaCl Solutions with Increasing Concentrations of Bile Salt Aggregates

conc (mM)	τ_1/ns[a] (a_1)	τ_2/ns[a] (a_2)	τ_3/ns[b] (a_3)	$\langle\tau_f\rangle$ (ns)	Φ_f	k_r (10^8 s^{-1})	k_{nr} (10^9 s^{-1})
			NaDC				
0	0.09 (0.99)		4.00 (0.01)	0.13	0.005	0.38	7.65
2	0.09 (0.96)	0.38 (0.03)	4.28 (0.01)	0.14	0.009	0.64	7.08
5	0.12 (0.54)	0.48 (0.44)	1.89 (0.02)	0.31	0.019	0.61	3.16
10	0.15 (0.46)	0.50 (0.52)	1.89 (0.02)	0.37	0.026	0.70	2.63
20	0.15 (0.43)	0.51 (0.55)	1.89 (0.02)	0.38	0.030	0.79	2.55
40	0.22 (0.48)	0.59 (0.50)	2.27 (0.02)	0.45	0.032	0.72	2.15
80	0.26 (0.54)	0.65 (0.44)	2.61 (0.02)	0.48	0.030	0.62	2.02
			NaC				
2	0.09 (0.99)		4.00 (0.01)	0.13	0.006	0.46	7.65
5	0.09 (0.93)	0.40 (0.06)	2.58 (0.01)	0.13	0.007	0.54	7.64
10	0.11 (0.70)	0.53 (0.29)	2.58 (0.01)	0.26	0.012	0.46	3.80
20	0.18 (0.47)	0.56 (0.52)	2.57 (0.01)	0.40	0.016	0.40	2.46
40	0.20 (0.43)	0.59 (0.56)	2.25 (0.01)	0.44	0.015	0.34	2.24
80	0.25 (0.51)	0.66 (0.48)	3.86 (0.01)	0.48	0.014	0.29	2.05
			NaTC				
2	0.09 (0.99)		4.00 (0.01)	0.13	0.006	0.46	7.65
5	0.09 (0.95)	0.47 (0.04)	4.00 (0.01)	0.14	0.007	0.50	7.09
10	0.12 (0.73)	0.60 (0.26)	4.00 (0.01)	0.28	0.011	0.39	3.53
20	0.17 (0.49)	0.61 (0.50)	3.05 (0.01)	0.42	0.016	0.38	2.34
40	0.20 (0.47)	0.65 (0.52)	2.29 (0.01)	0.45	0.014	0.31	2.19
80	0.28 (0.55)	0.70 (0.44)	3.37 (0.01)	0.50	0.013	0.26	1.97

[a]Uncertainty in measurements is ±0.01 ns. [b]Uncertainty in measurements ±0.25 ns.

around the probe molecules confined in the different bile salt aggregates. In this work, the location of HAN in the bile salt aggregates was confirmed by the time-resolved fluorescence anisotropy studies. In aqueous solution, the fluorescence anisotropy decay of HAN was found to be single-exponential in nature with the rotational relaxation time constant ~70 ps.[5] Gradual addition of bile salt to the aqueous solution of HAN leads to the biexponential anisotropy decay where the longer

dx.doi.org/10.1021/jp302435h | J. Phys. Chem. B 2012, 116, 8780−8792

time constant is attributed to the restricted rotational motion inside the hydrophobic nanocavities of bile salt aggregates. The anisotropy decays of HAN in different bile salt aggregates are given in Figure 5, and the fitted decay parameters are collected

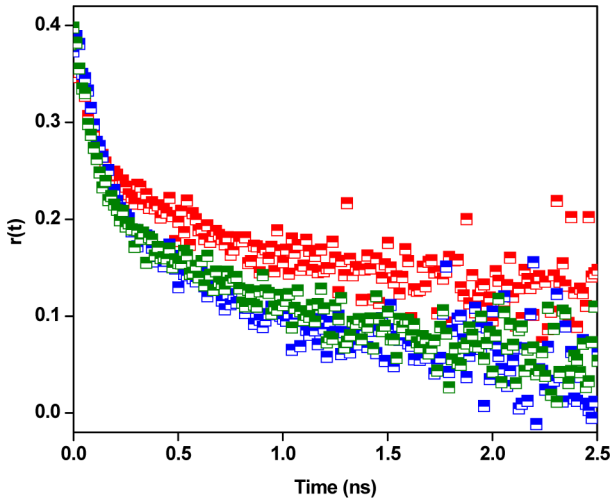

Figure 5. Fluorescence anisotropy decays of HAN in aqueous 0.2 M NaCl solutions of 40 mM NaDC (red), NaCh (blue), and NaTC (olive) (λ_{ex} = 375 nm, λ_{em} = 480 nm).

Table 3. Dynamic Parameters of Fluorescence Anisotropy of HAN in Aqueous 0.2 M NaCl Solutions of Different Bile Salt Aggregates

bile salt	conc (mM)	a_{1r}	τ_{1r} (ns)	a_{2r}	τ_{2r} (ns)	$\langle\tau_r\rangle$ (ns)[a]	χ^2
NaDC	40	0.25	0.09	0.75	0.95	0.73	1.02
NaC	40	0.30	0.09	0.70	0.89	0.65	1.11
NaTC	40	0.39	0.09	0.61	0.72	0.47	1.17

[a]Error in experimental data ±5%

in Table 3. The longer rotational relaxation times of HAN in the presence of all three bile salts compared to that of in water clearly indicate that HAN is located in a highly restricted microenvironment. The fluorescent anisotropy of a membrane-bound probe often does not decay to zero but reaches a constant nonzero value (r_∞).[73−75] This indicates that the rotational motion of the probe molecules is hindered. The anisotropy decay from its initial value (r_0) to the final value r_∞ can be expressed by a simple exponential function with rotational correlation time (τ_c)

$$r(t) = r_\infty + (r_0 - r_\infty)e^{-t/\tau_c} \quad (7)$$

Using DPH as a lipid-membrane-bound probe, Heyn[74] pointed out that, in anisotropic media, r_∞/r_0 is related to the order parameter (S) of the medium as

$$S^2 = \frac{r_\infty}{r_0} \quad (8)$$

The theoretical background of the order parameter has been discussed in several earlier reports.[73−75] Experimentally, the order parameter can be obtained from the relative contribution of the slow component, which is mainly responsible for the restricted rotational motion of the bound probe molecules. Therefore, to obtain better insight into the rotational restriction imposed on the probe molecules confined in the hydrophobic nanocavities of bile salt aggregates, we calculated the order parameters (S) using the equation

$$S^2 = a_{2r} \quad (9)$$

where a_{2r} is the relative amplitude of the slow component in the rotational relaxation decay parameters obtained from the time-resolved fluorescence anisotropy measurements. The value of the order parameter ranges from 0 to 1, where a value of 0 indicates no restriction and 1 means complete restriction of the rotational motion of the probe molecules. Therefore, the higher the value of the order parameter, the higher the rotational restriction, and hence, the higher the anisotropy values.

3.2. Effect of Sodium Chloride (NaCl). The excited-state properties of HAN are highly sensitive to the polarity of the microenvironment around the probe molecules, which is reflected in the significant changes in both the steady-state and time-resolved fluorescence properties when HAN is bound to bile salt aggregates, as discussed in the preceding sections.

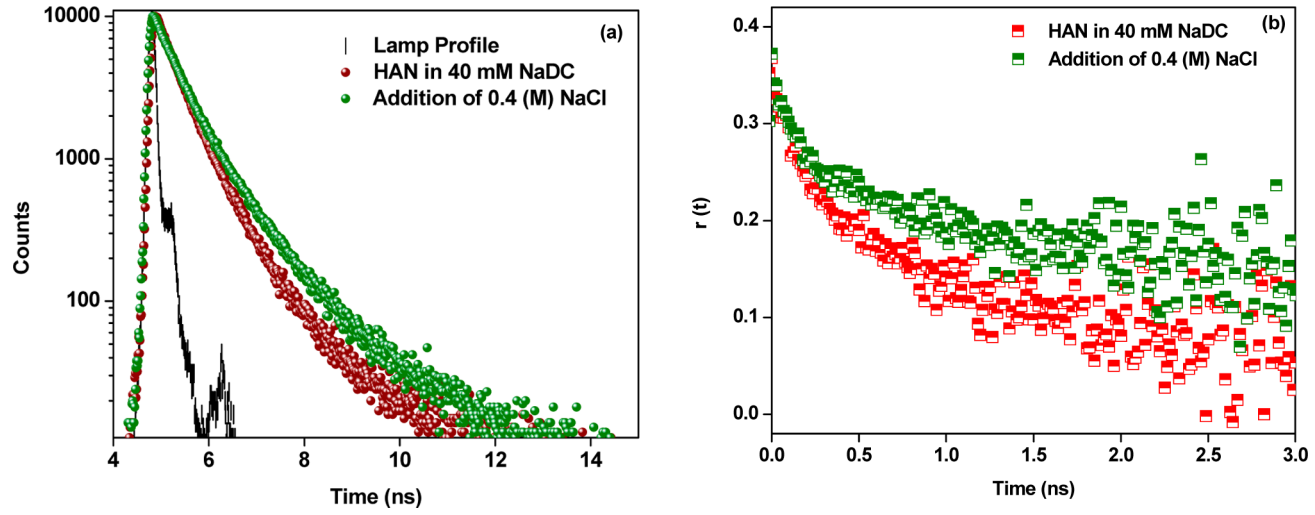

Figure 6. Effect of NaCl on time-resolved (a) fluorescence intensity decay and (b) anisotropy decay of HAN in aqueous solution of 40 mM NaDC (λ_{ex} = 375 nm, λ_{em} = 480 nm).

dx.doi.org/10.1021/jp302435h | J. Phys. Chem. B 2012, 116, 8780−8792

Table 4. Effect of NaCl on Fluorescence Lifetimes and Anisotropy Decay Parameters of HAN in Aqueous Solutions of NaDC (40 mM)[a]

	fluorescence lifetime decay parameters				fluorescence anisotropy decay parameters		
NaCl conc (M)	τ_1/ns (a_1)	τ_2/ns (a_2)	τ_3/ns (a_3)	$\langle\tau_f\rangle$ (ns)	τ_{1r}/ns (a_{1r})	τ_{2r}/ns (a_{2r})	$\langle\tau_r\rangle$ (ns)
0	0.20 (0.43)	0.54 (0.56)	2.18 (0.01)	0.41	0.09 (0.26)	0.88 (0.74)	0.67
0.2	0.22 (0.48)	0.59 (0.50)	2.27 (0.02)	0.45	0.09 (0.25)	0.95 (0.75)	0.73
0.4	0.22 (0.47)	0.67 (0.50)	2.25 (0.03)	0.51	0.09 (0.28)	1.14 (0.72)	0.85
0.6	0.27 (0.53)	0.74 (0.42)	2.39 (0.03)	0.53	–	–	–

[a]Error in experimental data = ±5%

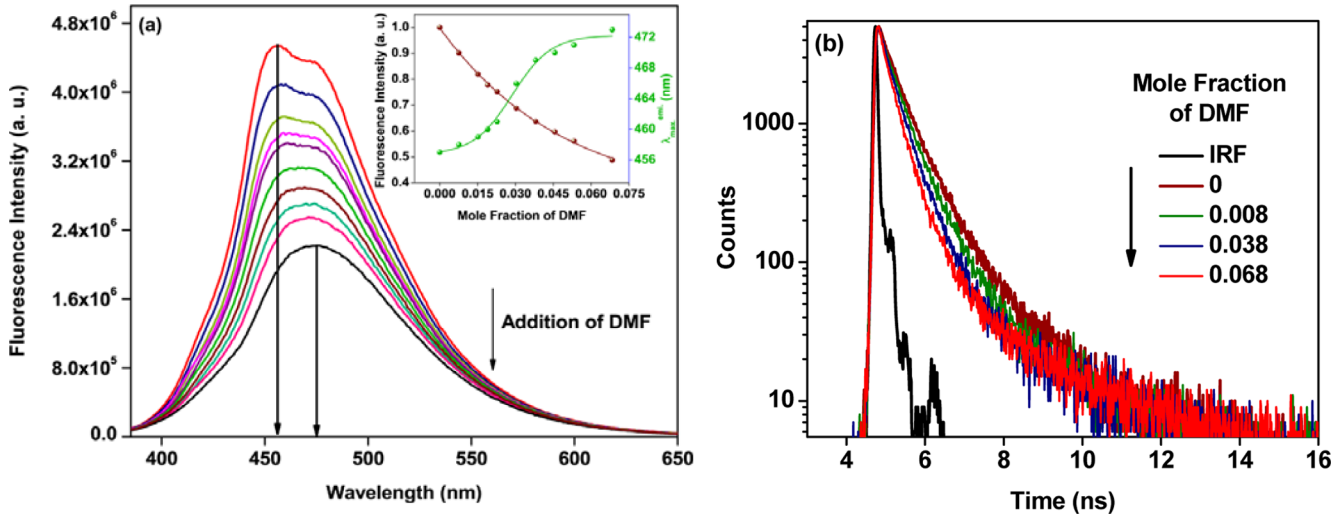

Figure 7. Effect of addition of DMF on the (a) steady-state fluorescence spectra (λ_{ex} = 375 nm) (inset: variation of emission intensity and λ_{max}^{emi} of HAN with increasing concentration of DMF) and (b) time-resolved fluorescence decay (λ_{ex} = 375 nm, λ_{em} = 480 nm) of HAN in aqueous solution of NaDC (80 mM).

This study also addressed the question of how salt-induced changes in the properties of bile salt aggregates, including size, shape, and polarity of the microenvironment, affect the PT dynamics of aggregate-bound HAN. The time-resolved emission decays of HAN in aqueous solution of 40 mM NaDC before and after addition of NaCl are shown in Figure 6a, and the lifetime values obtained from the biexponential fitting are reported in Table 4. The other decay curves in NaCh and NaTC aggregates to show the effect of NaCl are given in Figure S2 (Supporting Information) for comparison. The enhancement in the fluorescence lifetime clearly indicates the changes in the surrounding microenvironment of the bound guest in the presence of increasing concentrations of NaCl. To further probe the microenvironmental changes occurring upon the addition of NaCl, we measured the time-resolved fluorescence anisotropy of HAN (Figures 6b and S3, Supporting Information) upon gradual addition of NaCl to an aqueous solution of 40 mM bile salt. The experimental results suggest that the addition of NaCl increases the rigidity of the microenvironment, which results in an increase in the values of the rotational relaxation time (Table 4).

3.3. Effect of Organic Solvent. Steady-state and time-resolved fluorescence spectroscopic studies were performed in 0.08 M NaDC solution to establish how the changes in the polarity of the microenvironment of bile salt aggregates induced by the gradual addition of water-miscible organic cosolvent such as DMF affect the photophysics and photodynamics of aggregate-bound confined HAN. Figure 7 presents the steady-state and time-resolved fluorescence emission spectra of HAN in 80 mM NaDC solution with increasing concentration of DMF. From the steady-state experiments, one can see that addition of DMF to the aqueous solution of NaDC not only changed the fluorescence intensity but also changed the emission maximum and the shape of the spectrum. The change in the fluorescence intensity and emission maximum of HAN upon gradual addition of DMF is shown in the inset of Figure 7a for a better understanding of how the local environment of the confined HAN alters upon addition of a water-miscible organic cosolvent. The changes in the fluorescence lifetime values given in Table 5 further reveal the underlying reasons for the marked changes upon addition of cosolvent.

Table 5. Effects of Formamide on Fluorescence Decay Parameters of HAN in Aqueous Solutions of NaDC (80 mM)

mole fraction of DMF	τ_1/ns[a] (a_1)	τ_2/ns[a] (a_2)	τ_3/ns[b] (a_3)	$\langle\tau_f\rangle$ (ns)
0	0.26 (0.54)	0.65 (0.44)	2.61 (0.02)	0.48
0.008	0.25 (0.56)	0.60 (0.42)	2.97 (0.02)	0.45
0.015	0.25 (0.59)	0.58 (0.40)	3.17 (0.01)	0.41
0.023	0.22 (0.59)	0.54 (0.40)	3.30 (0.01)	0.38
0.038	0.23 (0.60)	0.52 (0.39)	3.34 (0.01)	0.37
0.053	0.20 (0.62)	0.48 (0.37)	3.31 (0.01)	0.33
0.068	0.19 (0.65)	0.45 (0.34)	3.27 (0.01)	0.31

[a]Uncertainty in measurements is ±0.01 ns. [b]Uncertainty in measurements ±0.10 ns.

dx.doi.org/10.1021/jp302435h | J. Phys. Chem. B 2012, 116, 8780−8792

4. DISCUSSION

Encapsulation of HAN within the hydrophobic nanocavities of bile salt aggregates is evident from the prominent changes observed in the UV−vis absorption and fluorescence spectra of HAN in the presence of all three bile salts (Figures 1 and 2). The increase in absorbance at ∼368 nm with increasing concentration of bile salts is a clear manifestation of the more hydrophobic environment provided by the primary aggregates of bile salts, which helps to solubilize the enol form (E-II) of HAN in the ground state, which is reported to be very nonpolar, having a dipole moment of ∼2.99 D.[58] The slight red shift in the absorption spectra (Figure S1, Supporting Information) can be rationalized by the disruption of intermolecular hydrogen bond involved with water molecules when HAN is incorporated into the hydrophobic pockets of the bile salt aggregates. Incorporation of HAN into the primary aggregates helps to increase the strength of the intramolecular hydrogen bond of the ground-state enol form by decreasing the number of water molecules involved in the intermolecular hydrogen bond, which, in turn, helps to increase the electronic conjugation and, hence, leads to a slight red shift. This observation is completely in line with the earlier observations in protein and other hydrophobic nanocavities.[68,69]

The polarity/dielectric properties and hydrogen-bonding ability of the solvent molecules play an important role in controlling the ESIPT process of HAN.[64] Weakening the intramolecular hydrogen bond through external hydrogen bonding with the solvent molecules can retard the ESIPT process, as has been observed for a number of PT probe molecules such as (hydroxyphenyl)benzazoles.[76−78] Therefore, encapsulation within the hydrophobic interior of the bile salt aggregates enhances the PT emission through reduced accessibility of polar solvents. However, the increment of the fluorescence intensity with increasing concentration of bile salts begins to level off after a certain concentration depending on the nature of the bile salt, which indicates the attainment of host−guest inclusion complexation equilibrium.

The blue shift in the emission maxima in the presence of different concentrations of bile salts clearly indicates that the micropolarity sensed by the aggregate-bound probe molecules is less than that in the bulk aqueous phase because such a blue shift was observed on changing the solvent from polar, protic solvent water (∼490 nm) to the nonpolar, aprotic solvent methyl cyclohexane (∼480 nm). For the three bile salts of varying hydrphobicity, the extent of the blue shift was found to be highest in NaDC, with the appearance of a sharp peak at ∼454 nm. However, the spectral appearances were quite similar for NaCh and NaTC with respective emission maxima at ∼460 and 462 nm. Because NaDC aggregates are relatively more hydrophobic in nature than aggregates of the other two bile salts, NaCh and NaTC, because of the presence of fewer hydroxyl groups in the chemical structure of NaDC, the PT emission was found to be more affected in the presence of NaDC.

The minimum concentration of bile salts require to start aggregation, which is known as the critical micelle concentration (cmc) depends on the structural characteristic of the bile salts, as well as the experimental conditions such as temperature, ionic strength, and pH of the medium. As primary aggregates are reported to be formed by hydrophobic interactions, aggregation occurs at a lower monomer concentration for comparatively more hydrophobic NaDC, followed in order by NaCh and NaTC.[79−82] This is supported by the fact that the alteration behavior in the emission spectra of HAN appeared at a lower concentration for NaDC than for NaCh and NaTC, in good agreement with the reported cmc ranges of 4−6 mM for NaDC and 12−16 mM for NaCh and NaTC.[82] This can easily be understood from the variations of the emission intensities and emission maxima as functions of bile salt concentration shown in the insets of Figure 2. In each plot of emission intensity and emission maximum as a function of bile salt concentration, an inflection point is observed that indicates the spectral alteration at the cmc of the corresponding bile salt.[82] Moreover, as the concentration of bile salt increased, the fluorescence quantum yield increased to saturation (Figure S4, Supporting Information) with the appearance of a point of inflection around the cmc range of the corresponding bile salt, and the increase in quantum yield was found to be higher in magnitude upon complexation with NaDC compared to NaCh and NaTC, which indicates a greater extent of penetration of HAN into the relatively more hydrophobic and rigid compartment of NaDC aggregates.

As mentioned earlier, the introduction of bile salt aggregates decreases the polarity of the surrounding microenvironment, which enhances the solubilization of the hydrophobic probe molecules and, consequently, the partitioning of the HAN, particularly into the more hydrophobic NaDC aggregates. Figure 3 compares the binding abilities of the three different bile salt aggregates as the slope of the corresponding line provides a measure of the partition coefficient value of HAN between the aggregated and aqueous systems. From the results (Table 1), it was found that the partition coefficient of HAN in NaDC aggregates was 2−3 times greater than that in the other two bile salt aggregates, suggesting a larger affinity of HAN toward the more hydrophobic environment of NaDC, as expected from the nonpolar nature of the closed enol form. In this situation, hydrophobic interactions can strengthen each other, and in fact, higher partitioning was observed for HAN in NaDC than in NaCh and NaTC. Partitioning of HAN into the hydrophobic nanocavities of bile salt aggregates further provides information on how much protection the bile salt aggregates can provide to the bound guest. By the term protection, we mean the efficiency of the host systems to protect the probe molecules from interactions with water. A higher extent of partitioning means that a greater number of probe molecules are inside the hydrophobic pocket, that is, fewer probe molecules are accessible to interact with water. Generally, the protection efficiencies of hosting systems are monitored by fluorescence quenching of the bound dye using an ionic quencher that prefers to reside mostly in the aqueous phase. Bohne and co-workers[11,12] extensively studied the binding dynamics of various organic guests into different bile salt aggregates of varying hydrophobicity. Using steady-state and time-resolved fluorescence quenching by nitrite and iodide ions as quenchers, they concluded that the protection ability of NaDC aggregates from the accessibility of ionic quenchers is greater than those of NaCh and NaTC aggregates. Greater protection efficiency means a greater extent of penetration and, hence, lesser extent of fluorescence quenching because of the lesser accessibility of the ionic quenchers to the bound guests.

Partitioning of HAN into the bile salt aggregates significantly reduced the solvent-assisted nonradiative decay channels present in the bulk aqueous phase, as reflected in the observation of longer fluorescence lifetimes (Table 2) of the bound probe. Moreover, confined water molecules involved in

intermolecular hydrogen bonding with the bile salt monomer can further help to reduce the nonradiative decay pathways. The effects of confined water molecules on the photophysics and photodynamics of a bound guest in hydrophobic nanocavities of micelles, vesicles, and cyclodextrins have been reported by a number of groups.[83−85] Organero and co-workers[64,67,68] described in detail how the radiative and nonradiative decay rate constants of the proton-transfer tautomer are influenced by the polarity, viscosity, and hydrogen-bonding ability in both neat homogeneous solvent and confined nanocavities such as cyclodextrins. Consistent with the earlier reports,[68,69] the major contributing 90-ps lifetime component observed in neat water was ascribed to the proton-transferred keto (K*) tautomer. The additional longer-lifetime component, on the other hand, in the presence of bile salts arose because of the caging of the tautomers of HAN. Notably, as the concentration of the bile salt increased, the relative contribution of the fast component gradually decreased, and the relative contribution of the longer-lifetime component increased depending on the extent of probe encapsulation. The alteration behavior in the time-resolved decay profile (Figure 4) can easily be understood from the sudden decrease in the relative amplitude of the fast component, responsible for free HAN in water, around the concentration ranges (cmc) of 2−5 mM for NaDC and 10−20 mM for NaCh and NaTC. An exactly opposite trend was observed for the amplitude of the longer-lifetime component. This observation is well correlated with the alteration in the steady-state fluorescence behavior at the reported cmc ranges of the three bile salts.[82]

It is especially noteworthy that the effect of bile salts on the excited-state properties of HAN strikingly differs from that of conventional surfactants such as sodium dodecyl sulfate (SDS), cetyltrimethylammonium bromide (CTAB), and *t*-octylphenoxypolyethoxyethanol (TX-100). The different fluorescent behaviors in bile salt aggregates and surfactants forming micelles arises because of the greater water accessibility of HAN in the latter case, where it is confined to the more polar Stern layer.[69] The additional feature that makes bile salt aggregates different from conventional surfactant assemblies is that, unlike for conventional surfactant assemblies, the structures of the aggregates depend on the size and shape of the guest molecules.[17,86,87]

Binding of the probe molecules into the hydrophobic nanocavities of bile salt aggregates restricts the rotational motion of the probe molecules, as confirmed by the observation of longer rotational relaxation time constants of HAN in bile salt aggregates (Table 3). Moreover, the confined water molecules in bile salt monomers might also play an important role in reducing the rotational motion of the probe molecules, which requires the breaking of the solvent network. From the results, it is evident that the rotational relaxation time constant value of HAN in the NaDC aggregates was significantly longer than those observed in the NaCh and NaTC aggregates. This observation is in line with the fact that HAN experiences a more hydrophobic and restricted environment because of the lower water accessibility in NaDC aggregates, followed in order by NaCh and NaTC aggregates. Moreover, NaDC aggregates are reported to be larger than NaCh and NaTC aggregates, which also supports the observation of longer time constant values for the rotational motion of the NaDC aggregate−bound probe molecules. Again, the calculated value of the order parameters for NaDC aggregates is ∼0.87, which is comparatively higher than the values obtained for the caging of the tautomers in NaCh and NaTC aggregates. This further implies the greater rigidity of NaDC aggregates imposed on the confined probe molecules compared to the other two bile salt aggregates.

Because the aggregation behavior of a bile salt is strongly influenced by the ionic strength of the surrounding medium, the binding dynamics of confined probe molecules is expected to be significantly affected by the gradual addition of NaCl to an aqueous solution of bile salt.[88−90] At lower concentrations of bile salt, HAN is only partially bound to the bile salt aggregates. However, at higher concentrations, equilibrium is reached, as confirmed from the time-resolved fluorescent measurements showing negligible changes in the time-resolved decay profile because of enhanced viscosity. Therefore, 40 mM aqueous bile salt solutions were used to study the effect of ionic strength on the excited-state binding dynamics of HAN. From the results (Table 4), it is evident that an increase in the NaCl concentration led to an increase in the fluorescence lifetimes of the caged tautomers of HAN because of the reduced polarity of the microenvironment. Recently, Fuentelba et al.[91] demonstrated the modulation of properties of binding sites and host−guest binding dynamics upon changing the ionic strength of the surrounding medium by the gradual addition of NaCl. They further suggested that addition of NaCl results in a decrease in the polarity of the binding sites, as confirmed by the decrease of the I/III ratio of confined pyrene.[91] It is well-known that, on increasing the ionic strength of a medium, the minimum concentration of bile salt required to initiate aggregation decreases and the size of the aggregates increases. However, the extent of size increase is more prominent for dihydroxy derivatives of bile salts such as NaDC compared to trihydroxy derivatives of bile salts such as NaC and NaTC.[88−90] Therefore, the binding dynamics of HAN inside the nanocavity of NaDC is expected to be more affected than that in NaTC. This can be supported by the fact that the extent of the increase in lifetime was found to be greater in NaDC aggregates than in NaCh and NaTC aggregates upon the addition of the same concentration of NaCl. It was also observed that, at low concentration (i.e., just below the cmc range of the bile salts), when no more aggregates of bile salts were present in aqueous solution, the steady-state emission spectra of HAN were broad and spectral nature, but the shape of the emission spectra changed dramatically with the enhancement of fluorescence intensity upon addition of NaCl. This observation is in good agreement with the fact that addition of NaCl forces bile salts to aggregate at low concentration. Time-resolved fluorescence anisotropy measurements (Figures 6b and S3, Supporting Information) further provide information on how much the rotational motion of confined probe molecules is hindered by the increased size of aggregates resulting from the addition of salt. Fuentelba et al.[91] determined the change in the size of perylene-bound sodium cholate aggregates upon the addition of NaCl from the obtained rotational relaxation time constants following the Stokes−Einstein relationship using the reported[92] nominal change in the viscosity of the solution upon addition of salt and found an increase in the hydrodynamics radius of the aggregates in correlation with the increased rotational relaxation time in the presence of NaCl.

It has been reported that addition of organic cosolvents such as DMF, acetonitrile, and methanol enhances the accessibility of water molecules to the nanocavities of bile salt aggregates, and DMF has been reported to be more effective in changing the microenvironment of aggregates compared to the other

dx.doi.org/10.1021/jp302435h | J. Phys. Chem. B 2012, 116, 8780−8792

cosolvents such as methanol and acetonitrile.[17,93] In fact, cosolvents significantly decrease the strength of the hydrophobic interactions between bile salt monomers, which helps to make the binding sites less rigid and more polar by enhancing the accessibility of water. This is supported by the observation of a decrease in the fluorescence intensity and a marked red shift of the fluorescence maximum of HAN upon the gradual addition of DMF as observed in Figure 7a. Moreover, the decrease in the fluorescence lifetime (Figure 7b and Table 5) further indicates that HAN experienced a more polar and hydrophilic microenvironment in the presence of DMF as a cosolvent. The reason for choosing a higher bile salt concentration for the study of the cosolvent effect was that, at such concentrations, aggregates are reported to persist to higher mole fractions of DMF.[17]

5. CONCLUSIONS

In this study, the combined effects of polarity, hydrogen-bonding ability, and nanoconfinement were investigated by the introduction of three different types of bile salt aggregates of varying hydrophobicity into aqueous solutions of HAN. The more rigid and hydrophobic confined environment provided by NaDC aggregates was found to modulate the excited-state binding dynamics to a greater extent, as confirmed by steady-state and time-resolved measurements. Moreover, the higher encapsulation efficiency of HAN in the primary aggregates of NaDC compared to those of NaCh and NaTC, as determined by the quantitative estimation of partition coefficients, resulted in maximum enhancement of fluorescence quantum yield. For all three bile salts, sharp changes in the fluorescence quantum yield were observed at the reported cmc range of the corresponding bile salt. Moreover, salt- and cosolvent-induced changes in the properties of the confined microenvironment, including the size, shape, and polarity of the aggregates, strongly affected the excited-state dynamics of HAN, as observed from the steady-state and time-resolved fluorescence experiments. On the basis of our experimental findings, we conclude that HAN can be utilized as a sensitive fluorophores to probe bile salt aggregates. The information obtained in this study will certainly be helpful in the further study of sensing and medicinal chemistry because bile salts have recently seen extensive use as vehicles for both hydrophobic and hydrophilic drug molecules.

■ ASSOCIATED CONTENT

Supporting Information

Information on the changes in the time-resolved fluorescence decays of HAN in NaCh and NaTC aggregates and other valuable information. This material is available free of charge via the Internet at http://pubs.acs.org.

■ AUTHOR INFORMATION

Corresponding Author

*E-mail: nilmoni@chem.iitkgp.ernet.in. Fax: 91-3222-255303.

Notes

The authors declare no competing financial interest.

■ ACKNOWLEDGMENTS

N.S. is thankful to the Council of Scientific and Industrial Research (CSIR) and the Board of Research in Nuclear Sciences (BRNS), Government of India, for generous research grants. S.M., S.G., and V.G.R. are thankful to CSIR for research fellowships. C.B. is thankful to UGC for a research fellowship.

■ REFERENCES

(1) Small, D. M. In *The Bile Salts*; Nair, P. P., Kritchevsky, D., Eds.; Plenum Press: New York, 1971; Vol. *1*, pp 249−256.
(2) O'Connor, C. J.; Wallace, R. G. *Adv. Colloid Interface Sci.* **1985**, *22*, 1−111.
(3) Borgtstorm, B.; Barrowman, J. A.; Lindstorm, M. In *Sterols and Bile Acid*; Danielsson, H., Sjoval, J., Eds.; Elsevier: Amsterdam, 1985.
(4) Douhal, A. *Chem. Rev.* **2004**, *104*, 1955−1976.
(5) Douhal, A. *Acc. Chem. Res.* **2004**, *37*, 349−355.
(6) Bhattacharyya, K. *Acc. Chem. Res.* **2003**, *36*, 95−101.
(7) Dsouza, R. N.; Pischel, U.; Nau, W. M. *Chem. Rev.* **2011**, *111*, 7941−7980.
(8) Bohne, C. Dynamics of Guest Binding to Supramolecular Assemblies. In *Supramolecular Photochemistry: Controlling Photochemical Processes*; Ramamurthy, V., Inoue, Y., Eds.; John Wiley & Sons: New York, 2011; Chapter 1.
(9) Ukeama, K.; Hirayama, F.; Irie, T. *Chem. Rev.* **1998**, *98*, 2045−2076.
(10) Xia, Y.; Rodgers, J.; Paul, K. E.; Whitesides, G. M. *Chem. Rev.* **1999**, *99*, 1823−1848.
(11) Li, R.; Carpentier, E.; Newell, Ed. D.; Olague, L. M.; Heafey, E.; Yihwa, C.; Bohne, C. *Langmuir* **2009**, *25*, 13800−13808.
(12) Amundson, L. L.; Li, R.; Bohne, C. *Langmuir* **2008**, *24*, 8491−8500.
(13) Ju, C.; Bohne, C. *J. Phys. Chem.* **1996**, *100*, 3847−3854.
(14) Wiedmann, T. S.; Liang, W.; Kamel, L. *Pharm. Res.* **2002**, *19*, 1203−1208.
(15) Mukhopadhyay, S.; Maitra, U. *Curr. Sci.* **2004**, *87*, 1666−1683.
(16) Cai, X.; Grant, D. J.; Wiedmann, T. S. *J. Pharm. Sci.* **1997**, *86*, 372−377.
(17) Megyesi, M.; Biczók, L. *J. Phys. Chem. B* **2007**, *111*, 5635−5639.
(18) Cabral, D. J.; Small, D. M. *Compr. Physiol.* **2011**, 621−662.
(19) Pattabiraman, M.; Kaanumalle, L. S.; Ramamurthy, V. *Langmuir* **2006**, *22*, 2185−2192.
(20) Pace, T. C. S.; Souza Júnior, S. P.; Zhang, H. T.; Bohne, C. *Photochem. Photobiol. Sci.* **2011**, *10*, 1568−1577.
(21) Kratohvil, J. P. *Adv. Colloid Interface Sci.* **1986**, *26*, 131−154.
(22) Small, D. M.; Penkett, S. A.; Chapman, D. *Biochim. Biophys. Acta* **1969**, *176*, 178−189.
(23) Bottari, E.; D'Archivio, A. A.; Festa, M. R.; Galantini, L.; Giglio, E. *Langmuir* **1999**, *15*, 2996−2998.
(24) Pártay, L. B.; Sega, M.; Jedlovszky, P. *Langmuir* **2007**, *23*, 12322−12328.
(25) Funasaki, N.; Fukuba, M.; Kitagawa, T.; Nomura, M.; Ishikawa, S.; Hirota, S.; Neya, S. *J. Phys. Chem. B* **2004**, *108*, 438−443.
(26) Baldridge, A.; Amador, A.; Tolbert, L. M. *Langmuir* **2011**, *27*, 3271−3274.
(27) Seth, D.; Chakraborty, A.; Setua, P.; Chakrabarty, D.; Sarkar, N. *J. Phys. Chem. B* **2005**, *109*, 12080−12085.
(28) Sen, S.; Dutta, P.; Mukherjee, S.; Bhattacharyya, K. *J. Phys. Chem. B* **2002**, *106*, 7745−7750.
(29) Chakraborty, A.; Chakrabarty, D.; Seth, D.; Hazra, P.; Sarkar, N. *Spectrochim. Acta A: Mol. Biomol. Spectrosc.* **2006**, *63*, 594−602.
(30) Adhikari, A.; Dey, S.; Mandal, U.; Das, D. K.; Ghosh, S.; Bhattacharyya, K. *J. Phys. Chem. B* **2008**, *112*, 3575−3580.
(31) Wu, J.; Liu, W.; Ge, J.; Zhang, H.; Wang, P. *Chem. Soc. Rev.* **2011**, *40*, 3483−3495.
(32) Sobolewski, A. L.; Domcke, W. *Phys. Chem. Chem. Phys.* **2006**, *8*, 3410−3417.
(33) Weller, A. H. *Z. Elektrochem.* **1952**, *56*, 662−668.
(34) Weller, A. H. *Prog. React. Kinet.* **1961**, *1*, 187−214.
(35) Beens, H.; Grellmann, K. H.; Gurr, M.; Weller, A. H. *Discuss. Faraday Soc.* **1965**, *39*, 183−193.
(36) Takeuchi, S.; Tahara, T. *J. Phys. Chem. A* **1998**, *102*, 7740−7753.
(37) Takeuchi, S.; Tahara, T. *J. Phys. Chem. A* **2005**, *109*, 10199−10207.

(38) Catalán, J.; Diaz, C.; Perez, P.; De Paz, L. G. *J. Phys. Chem. A* **2006**, *110*, 9116−9122.
(39) Adhikary, R.; Mukherjee, P.; Kee, T. W.; Petrich, J. W. *J. Phys. Chem. B* **2009**, *113*, 5255−5261.
(40) Chen, Y.; Gai, F.; Petrich, J. W. *J. Am. Chem. Soc.* **1993**, *115*, 10158−10166.
(41) Douhal, A.; Kim, S. K.; Zewail, A. H. *Nature* **1995**, *378*, 260−263.
(42) Gil, M.; Ziółek, M.; Organero, J. A.; Douhal, A. *J. Phys. Chem. C* **2010**, *114*, 9554−9562.
(43) Seo, J.; Kim, S.; Park, S. Y. *J. Am. Chem. Soc.* **2004**, *126*, 11154−11155.
(44) Solntsev, K. M.; Clower, C. E.; Tolbert, L. M.; Huppert, D. *J. Am. Chem. Soc.* **2005**, *127*, 8534−8544.
(45) Luiz, M.; Biasutti, A.; Soltermann, A. T.; Garcia, N. A. *Polym. Degrad. Stab.* **1999**, *63*, 447−453.
(46) Organero, J. A.; Garcla-Ochoa, I.; Moreno, M.; Lluch, J. M.; Santos, L.; Douhal, A. *Chem. Phys. Lett.* **2000**, *328*, 83−89.
(47) Catalán, J.; del Valle, J. C.; Diaz, C.; Palomar, J.; de Paz, J. L. G.; Kasha, M. *Int. J. Quantum Chem.* **1999**, *72*, 421−438.
(48) Douhal, A.; Lahmani, F.; Zehnacker-Rentien, A. *Chem. Phys.* **1993**, *178*, 493−504.
(49) Organero, J. A.; Moreno, M.; Santos, L.; Lluch, J. M.; Douhal, A. *J. Phys. Chem. A* **2000**, *104*, 8424−8431.
(50) Ortiz-Sánchez, J. M.; Gelabert, R.; Moreno, M.; Lluch, M. *J. Chem. Phys.* **2007**, *127*, 084318.
(51) Lochbrunner, S.; Schultz, T.; Schmitt, M.; Shaffer, J. P.; Zgierski, M. Z.; Stolow, A. *J. Chem. Phys.* **2001**, *114*, 2519−2522.
(52) Douhal, A.; Lahmani, F.; Zewail, A. *Chem. Phys.* **1996**, *207*, 477−498.
(53) Szeghalmi, A. V.; Engel, V.; Zgierski, Z. M.; Popp, J.; Schmitt, M. *J. Raman Spectrosc.* **2006**, *37*, 148−160.
(54) Lu, C.; Husieh, R. M. R.; Lee, I. R.; Cheng, P. Y. *Chem. Phys. Lett.* **1999**, *310*, 103−110.
(55) Tobita, S.; Yamamoto, M.; Kurahayashi, N.; Tsukagoshi, R.; Nakamura, Y.; Shizuka, H. *J. Phys. Chem. A* **1998**, *102*, 5206−5214.
(56) Catalán, J.; del Valle, J. C. *J. Am. Chem. Soc.* **1993**, *115*, 4321−4325.
(57) Catalán, J.; de Paz, J. L. G. *J. Phys. Chem. A* **2001**, *105*, 7315−7316.
(58) Catalán, J.; de Paz, J. L. G. *J. Phys. Chem. A* **2008**, *112*, 904−914.
(59) Paul, B. K.; Guchhait, N. *J. Phys. Chem. B* **2010**, *14*, 12528−12540.
(60) Paul, B. K.; Samanta, A.; Guchhait, N. *Langmuir* **2010**, *26*, 3214−3224.
(61) Singh, R. B.; Mahanta, S.; Kar, S.; Guchhait, N. *Chem. Phys.* **2007**, *331*, 373−384.
(62) Lochbrunner, S.; Szeghalmi, A.; Stock, K.; Schmitt, M. *J. Chem. Phys.* **2005**, *122*, 244315.
(63) Catalán, J.; Palomar, J.; De Paz, J. L. G. *Chem. Phys. Lett.* **1997**, *269*, 151−155.
(64) Organero, J. A.; Douhal, A. *Chem. Phys. Lett.* **2003**, *381*, 759−765.
(65) Organero, J. A.; Santos, L.; Douhal, A. In *Femtochemistry and Femtobiology: Ultrafast Dynamics in Molecular Science*; Douhal, A., Santamaria, J., Eds.; World Scientific: Singapore, 2002; p 225.
(66) Organero, J. A.; Tormo, L.; Douhal, A. *Chem. Phys. Lett.* **2002**, *363*, 409−414.
(67) Organero, J. A.; Douhal, A. *Chem. Phys. Lett.* **2003**, *373*, 426−431.
(68) Organero, J. A.; Martin, C.; Cohen, B.; Douhal, A. *Langmuir* **2008**, *24*, 10352−10357.
(69) Mandal, S.; Rao, V. G.; Ghatak, C.; Pramanik, R.; Sarkar, S.; Sarkar, N. *J. Phys. Chem. B* **2011**, *115*, 12108−12119.
(70) Selvam, S.; Mishra, A. K. *Photochem. Photobiol. Sci.* **2011**, *10*, 66−75.
(71) Seth, D.; Chakrabarty, D.; Chakraborty, A.; Sarkar, N. *Chem. Phys. Lett.* **2005**, *401*, 546−552.
(72) Rodrigues, C.; Gamerio, P.; Reis, S.; Lima, J. L. F. C.; Castro, B. D. *Langmuir* **2002**, *18*, 10231−10236.
(73) Lakowicz, J. R. *Principles of Fluorescence Spectroscopy*, 3rd ed.; Plenum Press: New York, 2006.
(74) Heyn, M. P. *FEBS Lett.* **1979**, *108*, 359−364.
(75) Birch, D. J. S.; Imhof, R. E. In *Topics in Fluorescence Spectroscopy*; Lakowicz, J. R., Ed.; Plenum Press: New York, 1991; Vol. *1*, pp 1−95.
(76) Sarkar, N.; Das, K.; Das, S.; Datta, A.; Nath, D.; Bhattacharyya, K. *J. Phys. Chem.* **1995**, *99*, 17711−17714.
(77) Elsaesser, T.; Schmetzer, B. *Chem. Phys. Lett.* **1987**, *140*, 293−299.
(78) Potter, C. A. S.; Brown, R. G. *Chem. Phys. Lett.* **1988**, *153*, 7−12.
(79) Roda, A.; Hofmann, A. F.; Mysels, K. J. *J. Biol. Chem.* **1983**, *258*, 6362−6370.
(80) Meyerhoffer, S. M.; McGown, L. B. *Langmuir* **1990**, *6*, 187−191.
(81) O'Connor, C. J.; Ch'ng, B. T.; Wallace, R. G. *J. Colloid Interface Sci.* **1983**, *95*, 410−419.
(82) Reis, S.; Moutinho, C. G.; Matosa, C.; de Castro, B.; Gameiroc, P.; Lima, J. L.F. C. *Anal. Biochem.* **2004**, *334*, 117−126.
(83) Bagchi, B. *Chem. Rev.* **2005**, *105*, 3197−3218.
(84) Pal, S.; Zewail, A. H. *Chem. Rev.* **2004**, *104*, 2099−2123.
(85) Mondal, J. A.; Nihonyanagi, S.; Yamaguchi, S.; Tahara, T. *J. Am. Chem. Soc.* **2010**, *132*, 10656−10657.
(86) Ju, C.; Bohne, C. *Photochem. Photobiol.* **1996**, *63*, 60−67.
(87) Waissbluth, O. L.; Morales, M. C.; Bohne, C. *Photochem. Photobiol.* **2006**, *82*, 1030−1038.
(88) Guveli, D. E. *Colloid Polym. Sci.* **1986**, *264*, 707−711.
(89) Hashimoto, S.; Thomas, J. K. *J. Colloid Interface Sci.* **1984**, *102*, 152−163.
(90) Garidel, P.; Hildebrand, A.; Neubert, R.; Blume, A. *Langmuir* **2000**, *16*, 5267−5275.
(91) Fuentelba, D.; Thurber, K.; Bovero, E.; Pace, T. C. S.; Bohne, C. *Photochem. Photobiol. Sci.* **2011**, *10*, 1420−1430.
(92) Kestin, J.; Khalifa, H. E.; Correia, R. J. *J. Phys. Chem.* **1981**, *10*, 71−87.
(93) Yihwa, C.; Quina, F. H.; Bohne, C. *Langmuir* **2004**, *20*, 9983−9991.